arXiv:hep-ex/0202007v1 1 Feb 2002

DESY 01-218
hep-ex/0202007

e^+e^- Physics at LEP and a Future Linear Collider [1]

Wolfgang Lohmann
DESY Zeuthen

December 7, 2001

Abstract

A summary of results obtained from e^+e^- annihilations at LEP is given. The precision measurements around the Z resonance, the results from charged gauge boson production and searches for new particles are reviewed. Particular emphasis is devoted to the Higgs boson. The prospects of an e^+e^- linear collider in the energy range of about 1 TeV are discussed.

---

[1] Based on lectures given at the International School-Seminar 'Actual Problems of Particle Physics' in Gomel, Belarus.

1. Introduction

Annihilations of electrons and positrons were a long time ago in particular the testing ground of Quantum Electrodynamics (QED), *e.g.* to test the 'point-likeness' of leptons in the couplings to the photon [1]. The first hints that electron interactions can proceed not only via a virtual photon came from neutrino scattering, having shown evidence for neutral currents [2]. These were interpreted as the exchange of a heavy neutral gauge boson Z. The discovery of the Z, together with the discovery of charged gauge bosons $W^{\pm}$ [3] was a great step to give credibility to the Standard Model (SM) [4], unifying the electromagnetic and weak interactions. The LEP accelerator [5] was designed to test the SM with high precision. The accuracy finally reached allowed the confirmation of the SM on the level of quantum corrections in e^+e^- annihilations on the Z resonance. After upgrading of the LEP accelerator with superconducting cavities, the beam energies were increased above the W-pair production threshold, and self couplings of gauge bosons [6] were studied. This new energy domain was accessible for the first time, and the data are used to search for the missing key-stone of the SM, the Higgs boson [7], and for unexpected phenomena. Since neither the Higgs boson nor new particles were found limits on their masses are derived.

The precision measurements at LEP favour a Higgs boson with a mass below 200 GeV. The ideal machine to study such a Higgs boson and to explore the mechanism of spontaneous symmetry breaking is a linear e^+e^- collider in the energy range up to one TeV. The physics potential of the TESLA project [8] is discussed.

2. LEP Accelerator and Experiments

The LEP accelerator, the largest facility for particle physics research, was taken into operation in 1989. The accelerator and storage ring had an circumference of about 27 km. Four experiments, called ALEPH, DELPHI, L3 and OPAL [9] were placed equidistant along the ring. In the first stage, from 1989 to 1995, electron and positron beams were accelerated to an energy of about 45 GeV and the Z resonance was measured with high precision. The peak luminosity of the machine reached about $10^{32}\mathrm{cm}^{-2}\mathrm{s}^{-1}$. Each of the experiments recorded about 5×10^6 Z decays. After 1995 the energy was enlarged in several steps to more then 100 GeV per beam, exploring a new energy domain of e^+e^- annihilations.

3. The Basic Process

The basic process is the annihilation of electrons and positrons into a fermion-antifermion pair, as depicted in Figure 1. In the case of a symmetric accelerator the laboratory system is the centre-of-mass system and the total energy of the annihilation, E_{tot}, is:

$$E_{tot} = 2E_b = \sqrt{s},$$

where E_b is the beam energy and s the square of the sum of the four momenta of the electron and the positron, p_{e^-} and

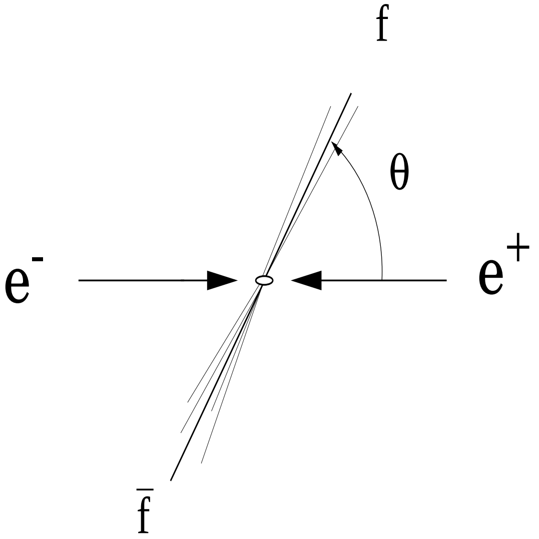

Figure 1: Schematic view of the e$^+$e$^-$ annihilation into a fermion-antifermion pair. In case the fermions are quarks they hadronise into jets.

p_{e^+},

$$s = (p_{e^-} + p_{e^+})^2 = 4E_b^2.$$

The polar angle of the outgoing fermion, θ, is obtained from the momenta of the outgoing fermion and the beam electron, $\wp_f$ and $\wp_{e^-}$,

$$cos\theta = \frac{1}{|\wp_f| \cdot |\wp_{e^-}|}(\wp_f \cdot \wp_{e^-}).$$

The lowest order Feynman-graph for e$^+$e$^-$ annihilations into f$\,\bar{\mathrm{f}}$ is shown in Figure 2. In QED the exchanged gauge boson V is the photon and the vertex function Γ equals to $Qe\gamma^\mu$, where Q is the charge of the fermion, e the unit charge and γ^μ are the Dirac matrices. The matrix element:

$$M \propto \frac{Qe^2}{s}(\bar{u}^e\gamma_\mu u^e)(\bar{u}^f\gamma^\mu u^f),$$

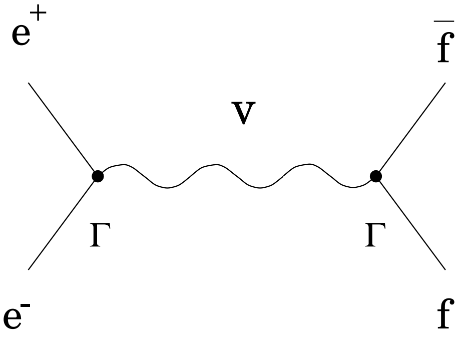

Figure 2: The Feyman-graph for e$^+$e$^-$ annihilation. V is the exchanged vector boson. The vertex functions are denoted as Γ.

where u^f are the four component spinors, leads then to the differential and total cross sections [2]

$$\frac{d\sigma}{d\Omega} = \frac{\alpha^2}{4s}(1 + cos^2\theta)$$

and

$$\sigma = \frac{4\pi\alpha^2}{3s}.$$

Here α is the 'fine structure' or electromagnetic coupling constant, $\alpha = e^2/4\pi$.

Assuming, instead of the photon, the exchange of a heavy neutral boson Z, the propagator term is replaced by a Breit-Wigner function. Allowing in addition a more general Lorentz structure, the vertex function is extended to $\Gamma = \gamma^\mu(v_f - a_f\gamma^5)$, introducing vector, v_f, and axial-vector, a_f, couplings of the neutral current. The matrix element reads then

$$\begin{aligned} M \quad \propto \quad & \frac{Qe^2}{s}\chi(s)(\bar{u}^e\gamma_\mu(v_e - a_e\gamma^5)u^e) \\ & (\bar{u}^f\gamma^\mu(v_f - a_f\gamma^5)u^f), \end{aligned}$$

---

[2] For annihilations into leptons Q=1.

where $\chi(s)$ is the Breit-Wigner function

$$\chi(s) = \frac{-G_{\mathrm{F}} \mathrm{m_Z}^2 s}{2\sqrt{2}\pi\alpha(s - \mathrm{m_Z}^2 + i\Gamma_Z \mathrm{m_Z})}.$$

Here G_{F} is the Fermi constant, $\mathrm{m_Z}$ the mass and Γ_Z the width of the Z boson. The cross sections obtained, allowing both photon and Z exchange, are:

$$\begin{aligned} \frac{d\sigma}{d\Omega} &= \frac{\alpha^2}{4s}(R(s)(1+\cos^2\theta) + \\ &\quad I(s)\cos\theta) \end{aligned}$$

and

$$\sigma = \frac{4\pi\alpha^2}{3s} R(s) \qquad (1)$$

with, in the case of leptons [3],

$$\begin{aligned} R(s) &= 1 + 2v_e v_f \Re(\chi(s)) + \\ &\quad (v_e^2 + a_e^2)(v_f^2 + a_f^2)|\chi(s)|^2 \\ I(s) &= 4a_e a_f \Re(\chi(s)) + \\ &\quad 8v_e v_f a_e a_f |\chi(s)|^2. \end{aligned}$$

The term $I(s)$ results from the interference of photon and Z and vector and axial-vector contributions to the Z exchange.

4. Standard Model parameters

The Lagrangian of the SM obeys the $SU(2) \otimes U_Y(1)$ gauge symmetry, giving rise to two gauge couplings, g' and g, as free parameters. Two additional free parameters result from the spontaneous symmetry breaking, the vacuum expectation value of the Higgs field, υ_0, and the parameter λ determining the Higgs potential. These quantities are related to couplings usually measured in the experiment:

$$\begin{aligned} \alpha &= \frac{1}{4\pi}\frac{g^2 g'^2}{g^2 + g'^2} = \frac{1}{137.0359895} \\ G_{\mathrm{F}} &= (\upsilon_0^2\sqrt{2})^{-1} \\ &= 1.166389 \times 10^{-5}\ \mathrm{GeV}^{-2} \\ \mathrm{m_Z} &= \frac{\sqrt{g^2 + g'^2}}{2}\upsilon_0. \end{aligned}$$

The measurement of the three quantities α, G_{F} and $\mathrm{m_Z}$ would allow us to determine three free parameters of the theory. The couplings α and G_{F} are measured in other experiments with errors of 4.5×10^{-8} [10] and 1.9×10^{-5} [11], respectively. The measurement of $\mathrm{m_Z}$ is the missing link at this point, and performed by the LEP experiments.

5. Mass and Width of the Z

In order to measure the mass and width of the Z, $\mathrm{m_Z}$ and Γ_{Z}, we look first on the cross section for Z exchange only. It can be written as:

$$\sigma_{\mathrm{Z}} = 12\pi \frac{\Gamma_{ee}\Gamma_{f\bar{f}}}{\mathrm{m_Z}^2} \frac{s}{(s - \mathrm{m_Z}^2)^2 + (\frac{s\Gamma_Z}{\mathrm{m_Z}^2})^2}.$$

The partial width, $\Gamma_{f\bar{f}}$, is related to the vector and axial-vector couplings:

$$\Gamma_{f\bar{f}} = \frac{G_F \mathrm{m_Z}^3}{6\pi\sqrt{2}}(a_f^2 + v_f^2).$$

The measurement of $\mathrm{m_Z}$ can be performed by measuring the cross section as function of $\sqrt{s}$ and performing a fit using Eqn.(1), where σ_Z is the dominant contribution in the resonance region. Bremsstrahlung, mainly off the initial state electrons, and other higher order corrections, which change the shape of the cross section, have to be taken into account. The theoretical framework used to describe the energy dependence of the cross section is given in the software codes ZFITTER [12] and TOPAZ0 [13]. As an example, the result from the OPAL experiment [14] for hadronic final states is given in Figure 3. The measurements of the cross section as function of $\sqrt{s}$ is well described by the fit using Eqn.(1), including radiative corrections, with m_Z, Γ_Z and the partial widths as free parameters. These measurements were done for the processes $e^+e^- \rightarrow \ell^+\ell^-$, with ℓ = e, μ or τ, and $e^+e^- \rightarrow$ hadrons by all LEP experiments. The results for m_Z are shown in Figure 4 [15]. They are in good agreement and combined equal to $m_Z = 91187.5 \pm 2.1$ MeV. In the combination errors common to all experiments, *e.g.* due to the uncertainty of the LEP beam energy, are taken into account. The measurement of m_Z has a precision of $2.2 \cdot 10^{-5}$, well comparable with the one of the Fermi constant G_F. The measurements of Γ_Z are also combined from all LEP experiments yielding $\Gamma_Z = 2.4952 \pm 0.0023$ GeV. Using the partial widths, $\Gamma_{f\bar{f}}$, the width of invisible decays, Γ_{inv}, is obtained as $\Gamma_{inv} = 499.0 \pm 1.5$ MeV. Within the SM this quantity is interpreted in terms of the number

---

[3] for quarks this has to be multiplied by a colour factor $N_c = 3$ and the quark charge must taken into account in the photon couplings.

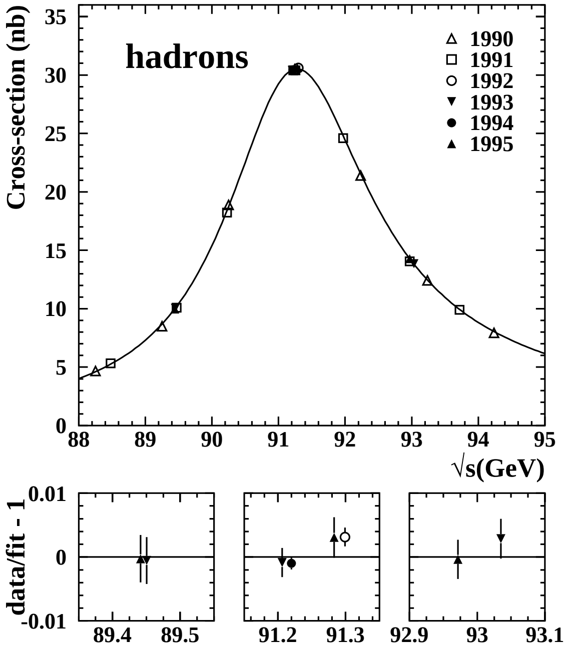

Figure 3: The cross section for e^+e^- annihilations into hadrons as function of the energy as measured by the OPAL collaboration. Also shown in the bottom plot is the deviation between data and fit.

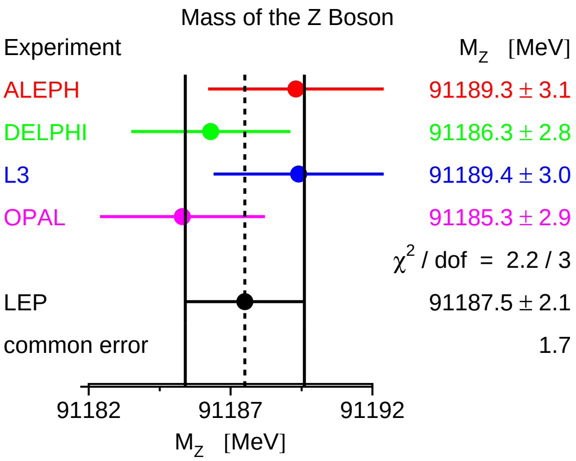

Figure 4: The results of the Z mass measurement by the four LEP experiments and their combination.

of neutrino species. The result is $N_\nu = 2.984 \pm 0.008$.

6. Couplings of the Z

In the SM the vector and axial-vector couplings of the Z to fermions are predicted as:

$$\begin{aligned} v_f &= I_3 - 2Q_{\mathrm{f}} s_W^2 \\ a_f &= I_3. \end{aligned}$$

Here I_3 is the third component of the weak isospin, Q_{f} the charge of the fermion and s_W the sinus of the electroweak mixing angle Θ_W. A prove of the SM is to compare these predictions to measurements.

The measurements are obtained using the total cross section, where σ_Z depends on a_f and v_f, the differential cross section $d\sigma/d\cos\theta$ and polarisation asymmetries.

Defining the forward-backward asymmetry, $\mathcal{A}_{FB}$, as the normalised difference of the cross sections integrated between $-1 < \cos\theta < 0$ and $0 < \cos\theta < 1$, respectively, one obtaines on the peak of the resonance:

$$\begin{aligned} \mathcal{A}_{FB} &= \frac{\sigma_F - \sigma_B}{\sigma_F + \sigma_B} \\ &= \frac{3}{4} \frac{v_e a_e}{v_e^2 + a_e^2} \frac{v_f a_f}{v_f^2 + a_f^2} \\ &= \frac{3}{4} \mathcal{A}_e \mathcal{A}_f. \end{aligned}$$

From the measurement of $\mathcal{A}_{FB}$ the product $\mathcal{A}_e \mathcal{A}_f$ can be determined.

The measurement of $\mathcal{A}_{FB}$ is done for the leptonic final states, for b- and c-quarks separately and averaged over all quarks. As an example, $\mathcal{A}_{FB}$ measured in $e^+e^- \to \mu^+\mu^-$ as a function of $\sqrt{s}$ by the DELPHI experiment [16] is shown in Figure 5. The points are the data at several $\sqrt{s}$ and the curve is the result of a fit using ZFITTER. In the lower plot the difference between the data and the fitted curve is also shown.

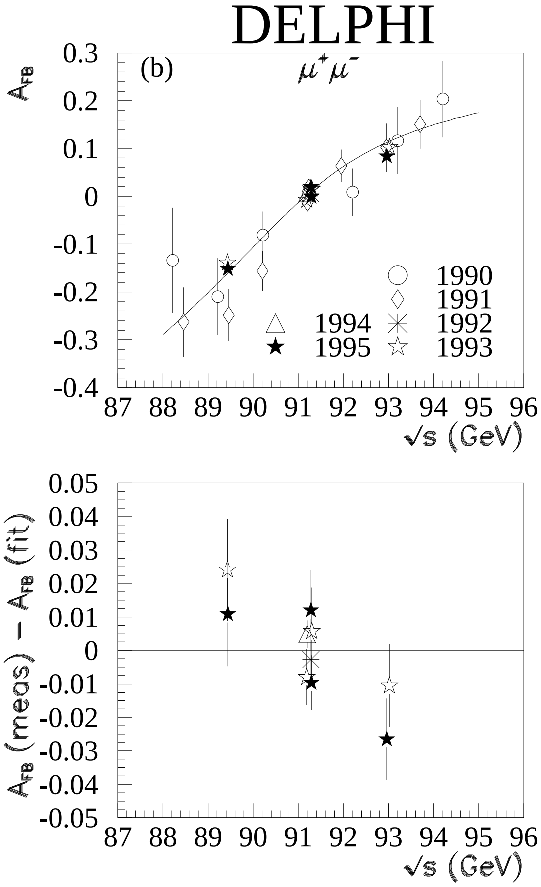

Figure 5: The results of the measurement of $\mathcal{A}_{FB}$ in $e^+e^- \to \mu^+\mu^-$ by the DELPHI collaboration.

More information about the couplings is obtained by the measurement of the polarisation of the fermions in the final state. Denoting with h_f the helicity of the final state fermion one obtains for unpolarised beams :

$$\begin{aligned}\mathcal{P} &= \frac{\sigma(h_f=+1)-\sigma(h_f=-1)}{\sigma(h_f=+1)+\sigma(h_f=-1)} \\ &= -\frac{2v_f a_f}{v_f^2+a_f^2} = -\mathcal{A}_f\end{aligned}$$

and

$$\mathcal{P}_{FB} = -\frac{4v_e a_e}{v_e^2+a_e^2} = -2\mathcal{A}_e.$$

$\mathcal{P}_{FB}$ denotes the forward-backward polarisation asymmetry. As can be seen, the measurement of the polarisation of the final state fermion allows to determine, separately for the electron and the final state fermion, the product of vector and axial-vector couplings.

In the experiments the polarisations are only accessible in the process $e^+e^- \rightarrow \tau^+\tau^-$, because the τ lepton has a very short lifetime and decays inside the detector. From the analysis of the τ decay products, assuming (V-A) structure of the charged current, the polarisation of the τ is measured. Also these measurements were done by all LEP collaborations and as an example the result of the L3 experiment [17] is shown in Figure 6. Taking the measurements of cross sections, forward-backward asymmetries and the measurement of the τ polarisation together, and using also $\mathcal{A}_{LR}$[4] from SLD [18], the vector and axial-vector couplings of the leptons are determined. This is shown in Figure 7 first for each lepton flavour separately. As can be seen, the couplings of electrons, muons and taus are in agreement, supporting the fundamental assumption of lepton universality.

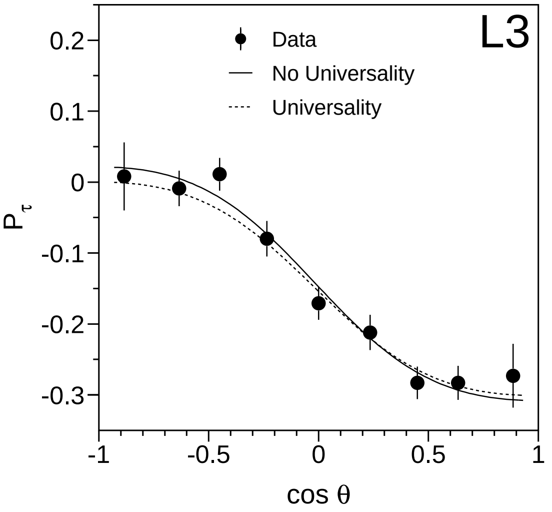

Figure 6: The polarisation of the τ in $e^+e^- \rightarrow \tau^+\tau^-$ as function of $\cos\theta$ measured by the L3 experiment.

7. Electroweak radiative corrections

Before interpreting the results on the couplings the phenomenon of electroweak loop corrections should be discussed. From QED the vacuum polarisation, described by fermion loops, is well known. Such corrections depend on the mass of the fermions and can easily calculated for leptons for which masses are precisely known. For quarks they are calculated from the low energy cross sections $e^+e^- \rightarrow$ hadrons via dispersion relations [19]. The vacuum polarisation leeds to an increase of the effective electromag-

---

[4] $\mathcal{A}_{LR} \sim \mathcal{A}_e$ is the cross section asymmetry for left-handed and right-handed electrons in e^+e^- annihilations measured with the polarised electron beam at SLAC.

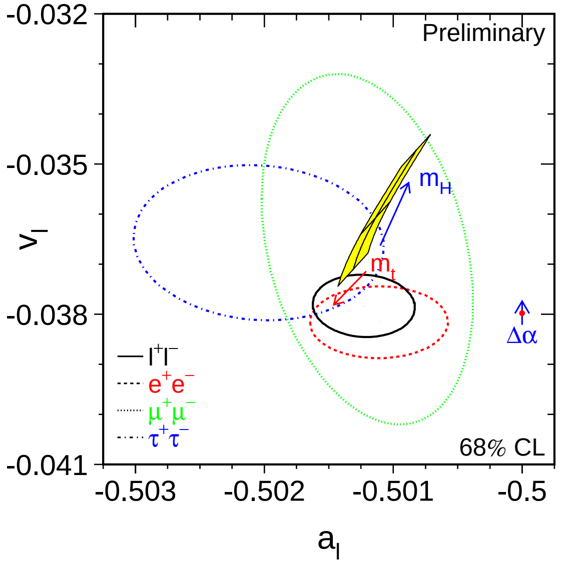

Figure 7: Lepton couplings determined by the LEP experiments and the measurement of $\mathcal{A}_{LR}$ from SLD [15].

netic coupling with s and at an energy corresponding to the Z mass this results in $\alpha(\mathrm{m_Z}^2) = \frac{\alpha(0)}{1-\Delta\alpha(\mathrm{m_Z}^2)} = 1./128.945$. In addition there are weak loop corrections, for which examples are shown in Figure 8. These corrections are quantified as Δr_W in the relation

$$G_\mathrm{F} = \frac{\pi\alpha}{\sqrt{2}\mathrm{m_W}^2 s_W^2}\frac{1}{1-\Delta\alpha(s)-\Delta r_W},$$

where $\mathrm{m_W}$ is the mass of the W boson. The upper diagram of Figure 8 results in contributions to Δr_W proportional to $\simeq \mathrm{m_t^2/m_W^2}$, where $\mathrm{m_t}$ is the mass of the top-quark. In addition, there are bosonic loops containing the Higgs boson. They are proportional to $\simeq ln\ \mathrm{m_H^2/m_W^2}$ [20].

In order to compare the measured couplings to the predictions of the theory,

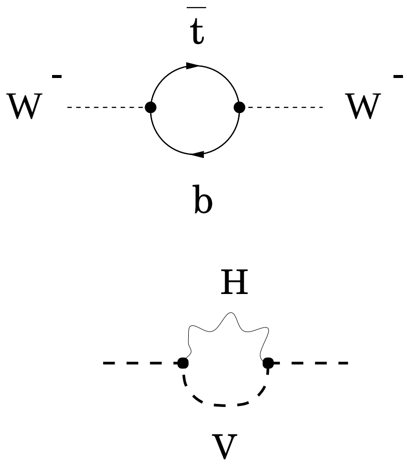

Figure 8: Lowest order weak correction diagram containing fermion loops (top) or the Higgs boson (bottom). V is either Z or W.

the improved Born approximation [21] is used, in which the electroweak loop corrections are absorbed in effective couplings:

$$\begin{aligned}\tilde{v}_f &= \sqrt{\rho}(I_3 - 2\kappa s_W^2)\\ \tilde{a}_f &= \sqrt{\rho}I_3.\end{aligned}$$

Here ρ [22] is the ratio of neutral to charged current couplings, $\rho = c_w^2\mathrm{m_Z}^2/\mathrm{m_W^2}$. At Born level holds $\rho = 1$. Weak loop corrections lead to $\rho = 1 + \Delta\rho$, with $\Delta\rho = -\frac{s_W^2}{c_W^2}\Delta r_W - \Delta r_{rem}$. The quantity Δr_{rem} containes non-leading contributions. In addition, weak loop corrections, similar in size, contribute to κ.

The exploitation of these relations was very successful at LEP before the discovery of the top-quark. Using the precision measurements around the Z, the $\simeq \mathrm{m_t^2/m_W^2}$ dependence of the weak loop contributions allowed to predict the top-quark mass in 1993 to be $\mathrm{m_t} = 166^{+17+19}_{-19-22}$ [23], in excellent agreement with the measurement after the discovery 1995 [24].

As shown in Figure 7, lepton universality is supported by the measurements. Hence the results from the leptonic final states are combined to derive universal lepton couplings. The result, also shown in Figure 7, leads to a value of a_l clearly differerent from the prediction of the SM of -0.5, pointing to significant contributions from weak corrections. Interpreting the measurements in the improved Born approximation the value of ρ is determined to be 1.0050 ± 0.0010 [15], different from unity by 5 standard deviations.

Using, in addition to LEP and SLD data, also results on $\mathrm{m_W}$ [25] and $\mathrm{m_t}$ [26] from the Tevatron and on atomic parity violation [27] a fit in the framework of the SM is performed with $\mathrm{m_H}$ as free parameter. In Figure 9 the dependence of the χ^2 of the fit on the mass of the Higgs boson is shown. The value for the Higgs boson mass obtained is $\mathrm{m_H} = 88^{+53}_{-35}$ GeV, or, at 95% C. L., $\mathrm{m_H} < 196$ GeV. Also shown in the Figure is the light grey area excluded from direct searches of the Higgs boson. Apparently, the electroweak precision measurements favour a light Higgs boson which might be just a bit above the current lower mass limit from direct searches.

8. e^+e^- annihilations above the Z

After 1995 the beam energy of the LEP accelerator was enlarged in several steps up to 104.5 GeV, reached in the year 2000. In addition to the annihilation into fermion-antifermion pairs we expect several new channels kinematically allowed and subject of new kind of studies. These are:

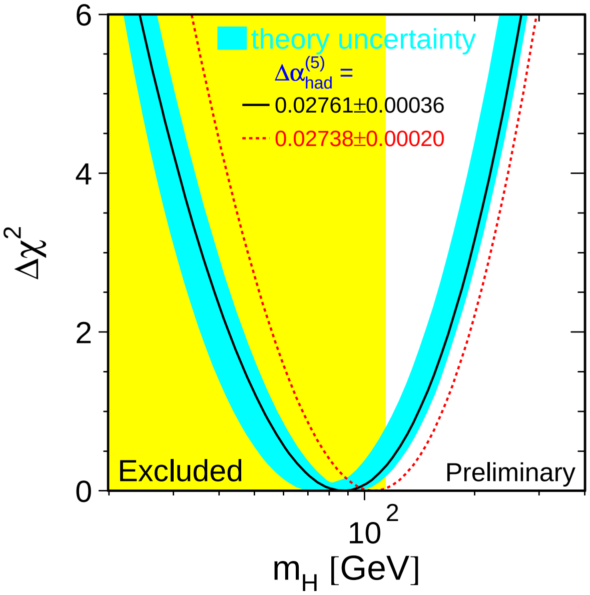

Figure 9: The χ^2 of a fit to all electroweak measurements with the Higgs boson mass as free parameter [15].

- $e^+e^- \to W^+W^-$: The pairwise production of W bosons allows the measurement of their mass, and, for the first time under very clean conditions, the study of triple gauge boson couplings.
- $e^+e^- \to ZZ$: In the SM this process is mediated by virtual electron exchange in the t-channel. The cross section is sensitive to anomalous gauge boson couplings.

- $e^+e^- \rightarrow$ Z H: This process is expected in the Standard Model. But since the mass of the Higgs boson is unknown, we do not know, whether it is accessible at LEP energies.
- $e^+e^- \rightarrow$ new particles: If there is physics beyond the Standard Model it can manifest itself *e.g.* via pair production of supersymmetric particles.

8.1. $e^+e^- \rightarrow f\,\bar{f}(\gamma)$

This process is mediated by virtual photon or Z exchange. Some fraction of the events is characterised by the radiation of a high energy photon in the initial state, reducing the effective annihilation energy to the mass of the Z. Of interest are, of course, the events where the annihilation happens with the full energy. The cross sections measured at high energy for $e^+e^- \rightarrow$ hadrons, $e^+e^- \rightarrow \mu^+\mu^-$ and $e^+e^- \rightarrow \tau^+\tau^-$ are shown in Figure 10 [28] for the fraction with full annihilation energy. The full lines are the expectations from the SM. As can be seen, the SM describes perfectly the dependence of the annihilation cross section on $\sqrt{s}$. These results are used to derive limits on new physics scales, *e.g.* the scale of contact interactions [29]. Such interactions are excluded up to several TeV [28] for any helicity structure of the amplitudes. Also stringent limits on couplings and masses of leptoquarks or additional heavy gauge bosons are derived from these measurements. For example, a sequential heavy gauge boson is excluded up to a mass of 1.89 TeV.

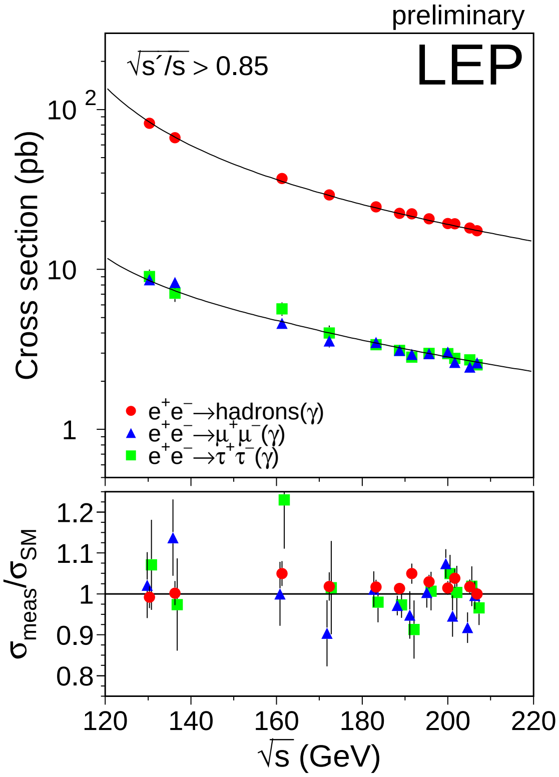

Figure 10: The cross section measurements for the processes $e^+e^- \rightarrow$ hadrons and $e^+e^- \rightarrow \ell^+\ell^-$ (ℓ =e, μ), at high energies combined for all LEP experiments.

8.2. W production and decay

Both single and pair production of W bosons are new physics topics at high energies. From $e^+e^- \rightarrow W^+W^-$ and $e^+e^- \rightarrow W^+e^-\overline{\nu}$ the mass of the W, m_W, the width of the W, and the couplings between gauge bosons, WWγ and WWZ, are measured.

The event topologies we expect for a W^+W^- final state are four jets when both W decay into quarks, $W \rightarrow q\bar{q}'$, two jets and one charged lepton when one W decays into quarks and the other into leptons, W → $\ell\nu$, or two charged leptons if both W decay leptonically.

The mass of the W is determined from the direct reconstruction of the invariant mass of the two jets or the two leptons. In the latter case the momentum of the neutrino is taken as the missing momentum of the event. An example for a such reconstructed mass distribution is shown in Figure 11 for the final state $q\bar{q}e\nu$ [30]. The distribution shows a clear, nearly background free, resonance shape. The measurement is done using all channels and the results of the LEP experiments are given in Figure 12. Combining them $m_W = 80.450 \pm 0.039$ GeVis obtained.

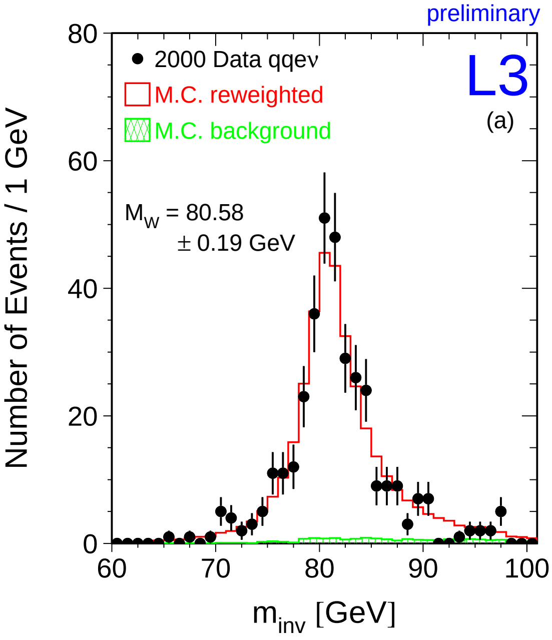

Figure 11: The measurement of the W mass by the L3 experiment in the final state $q\bar{q}'e\nu$.

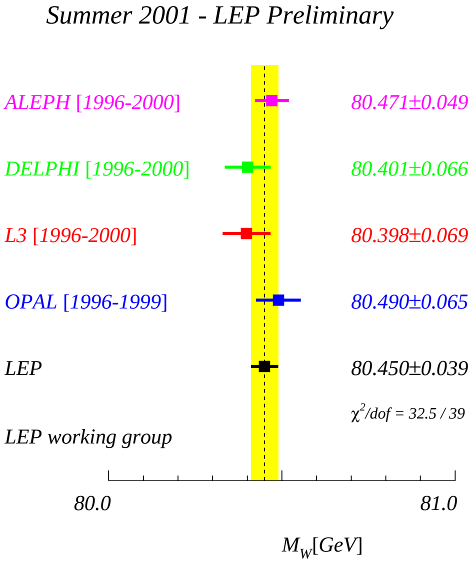

Figure 12: The measurement of the W mass by the LEP collaborations and their combination [15].

The process $e^+e^- \rightarrow W^+W^-$ is of particular interest because triple gauge boson couplings [6], predicted in non-abelian gauge theories, can be measured. In the SM three diagrams as shown in Figure 13 contribute to $e^+e^- \rightarrow W^+W^-$. Of particular interest are the latter two, because only they contain triple gauge boson couplings. Furthermore, the cross section obtained from each diagram sepa-

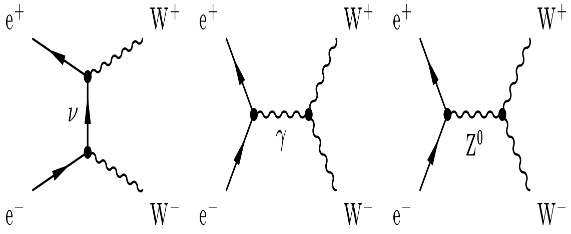

Figure 13: The processes contributing to $e^+e^- \rightarrow W^+W^-$.

rately is divergent with growing $\sqrt{s}$; only the sum of the three diagrams results in a finite cross section.

The measurements of the cross sections and the predicted behaviour for only neutrino exchange, neutrino plus photon exchange and and the sum of all contributions is shown in Figure 14. The data clearly favour the SM prediction. The γWW and ZWW vertices are described by 2×7 independent form factors [6]. Assuming CP and P conservation and electromagnetic gauge invariance, five independent couplings are left, $g_1^Z, \kappa_\gamma, \kappa_Z, \lambda_\gamma$ and λ_Z, with values predicted in the SM of 1, 1, 1, 0 and 0. The first coupling is $g_1^Z = \frac{g_{ZWW}}{g_{ZWW}^{SM}}$, with $g_{ZWW}^{SM} = g' c_W$ and the other quantites are related to static properties of the W, *e.g.* the magnetic dipole moment $\mu_W = \frac{e}{2\mathrm{m_W}}(1+\kappa_\gamma+\lambda_\gamma)$ or the electromagnetic quadrupole moment $Q_W = \frac{-e}{\mathrm{m_W^2}}(\kappa_\gamma - \lambda_\gamma)$. Assuming $SU(2)$ gauge invariance, the following relations hold:

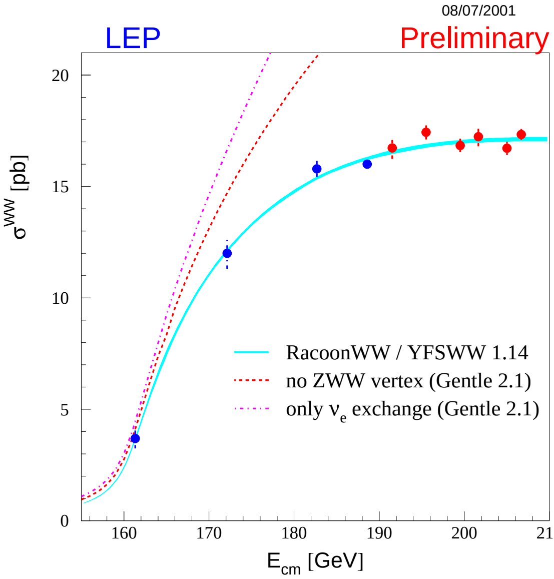

Figure 14: The cross section measurements for $e^+e^- \rightarrow W^+W^-$ and the predictions of the several subprocesses [15].

$$\begin{aligned}\Delta\kappa_Z &= \Delta g_1^Z \Delta\kappa_\gamma \tan^2\Theta_W \\ \lambda_Z &= \lambda_\gamma,\end{aligned}$$

where $\Delta\kappa$ and Δg_1^Z denote the deviation of the quantities from the SM value. Exploiting the total cross section measurements, the production and decay angular distributions of the W bosons and using also the measurements from single W production the three left parameters are determined. Fits, in which one parameter is free and the other two are set to their SM values, yield [31]:

$$\begin{aligned}\Delta g_1^Z &= -0.025 \pm 0.026, \\ \Delta\kappa_\gamma &= -0.002 \pm 0.067, \\ \lambda_\gamma &= -0.036 \pm 0.028.\end{aligned}$$

The results of two-dimensional fits give similar results, being in agreement with the SM expectations.

9. Searches

9.1. Higgs boson phenomenology

The Higgs mechanism is introduced to allow particles to acquire mass keeping the gauge invariance of the SM Lagrangian. In its minimal version a $SU(2)$ doublet of complex fields is introduced:

$$\Phi = \begin{pmatrix}\Phi_1(x)\\ \Phi_2(x)\end{pmatrix}.$$

The simplest Lagrangian reads

$$\mathcal{L}_H = \partial_\nu\Phi^\dagger\partial^\nu\Phi - \mathcal{V}(\Phi),$$

with the following choice of the potential

$$\mathcal{V}(\Phi) \;=\; -\mu^2\Phi^\dagger\Phi + \lambda(\Phi^\dagger\Phi)^2.$$

The state with minimal energy corresponds to the minimum of the potential. Defining

$$\frac{\upsilon}{\sqrt{2}} = \sqrt{\Phi^\dagger\Phi},$$

the potential reads:

$$\mathcal{V}(\Phi) = -\frac{1}{2}\mu^2\upsilon^2 + \frac{1}{4}\lambda\upsilon^4.$$

The minimum of the potential is reached at $\upsilon = \upsilon_0 = \sqrt{\mu^2/\lambda}$. This is illustrated in Figure 15. In the plane Φ_1 vs. Φ_2 the minimum of the potential is continously degenerated. The choice

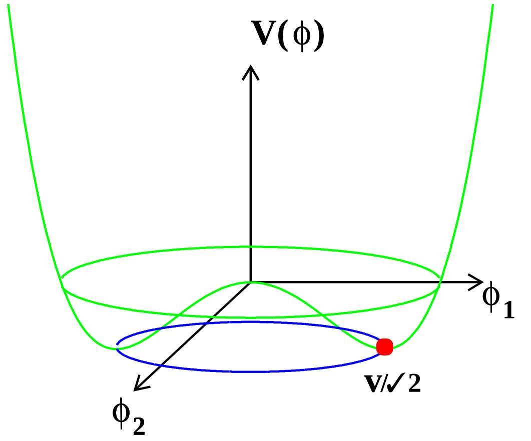

Figure 15: The shape of the potential of the Lagrangian describing the scalar $SU(2)$ doublet.

$$\Phi_0 = \begin{pmatrix} 0 \\ \frac{1}{\sqrt{2}}\upsilon_0 \end{pmatrix},$$

leads to a ground state, which is, in contrary to the potential, not invariant under $SU(2)$ transformations, a feature denoted as spontanous symmetry breaking. After redefinition of the scalar field, $H(x) = \upsilon(x) - \upsilon_0$, we inspect the covariant terms of the Lagrangian

$$\mathcal{L}_H \;=\; \mathcal{D}_\nu\Phi^\dagger\mathcal{D}^\nu\Phi - \mathcal{V}(\Phi).$$

It results into expressions

$$\frac{1}{4}g'^2\upsilon_0^2(W_\lambda^- W^{+\lambda})$$

and

$$\frac{1}{8}(g^2 + g'^2)\upsilon_0^2 Z_\lambda Z^\lambda,$$

which we interprete as mass terms for the W and Z bosons:

$$\begin{aligned} \mathrm{m}_\mathrm{W}^2 \;&=\; \frac{1}{4}g'^2\upsilon_0^2 \\ \mathrm{m_Z}^2 \;&=\; \frac{1}{4}(g^2 + g'^2)\upsilon_0^2. \end{aligned}$$

The interaction between gauge bosons and the Higgs boson is described by the terms:

$$\frac{1}{2}g'^2\upsilon_0(W_\lambda^- W^{+\lambda})H$$

and

$$\frac{1}{4}(g^2 + g'^2)\upsilon_0(Z_\lambda Z^\lambda)H.$$

In addition, there appear the terms $2\lambda\upsilon_0^2H^2$, $\lambda\upsilon_0H^3$ and $\frac{1}{4}\lambda H^4$. The first is the mass term of the physical state of the scalar field, the Higgs boson, with $\mathrm{m}_\mathrm{H}^2 = 2\lambda\upsilon_0^2$. The other two correspond to self couplings of the Higgs field. The parameter υ_0, the value of the potential in the ground state, is known from the measurement of G_F to be $\upsilon_0 \simeq 246$ GeV.

The parameter λ, determining the shape of the potential, appears in the mass term for the Higgs boson and in addition in the self couplings.

The discovery of the Higgs boson and the measurement of its mass will be the 'key-stone' of the SM. The measurement of the self couplings would confirm the shape of the potential as shown in Figure 15. Also terms describing quartic interactions between gauge bosons and Higgs bosons, not discussed here, appear.

The masses of the fermions are obtained from separately introduced Yukawa terms, *e.g.* for electrons, as

$$\begin{aligned}\mathcal{L}_Y &= \sqrt{2} g_{\mathrm{He^+e^-}} \bar{\mathrm{e}}_{\mathrm{R}} \Phi^\dagger \begin{pmatrix} \nu_{\mathrm{e}} \\ \mathrm{e_L} \end{pmatrix} + \mathrm{h.c.} \\ &= g_{\mathrm{He^+e^-}} \upsilon_0 (\bar{\mathrm{e}}_{\mathrm{L}} \mathrm{e_R} + \bar{\mathrm{e}}_{\mathrm{R}} \mathrm{e_L})\end{aligned}$$

with $m_e = g_{\mathrm{He^+e^-}} \upsilon_0$.

9.2. Higgs boson search

The production of the Higgs boson in $\mathrm{e^+e^-}$ annihilations proceeds at LEP energies dominantly via the Higgs-strahlung, illustrated in Figure 16. Higgs-strahlung reaches at a given centre-of-mass energy the kinematic limit if $\mathrm{m_H}+\mathrm{m_Z}$ approaches $\sqrt{s}$. The fusion process contributes below the kinematic threshold of the Higgs-strahlung only with a very small fraction to the cross section. This can be seen from Figure 17. Since the integrated luminosity of LEP at the highest energies, shown in Figure 18, is about 100 pb^{-1}, only the Higgs-strahlung is of practical importance.

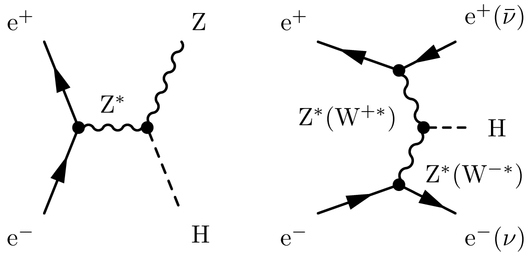

Figure 16: The production mechanisms of the Higgs boson at LEP: Higgs-strahlung(left) and fusion (right).

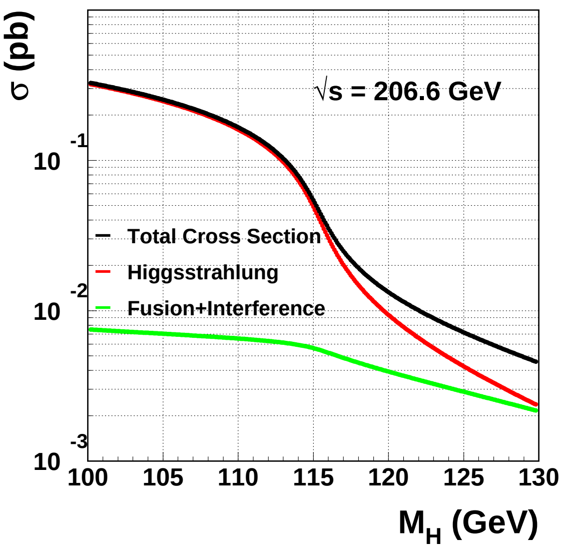

Figure 17: The cross sections of Higgs-strahlung and fusion processes at a centre-of-mass energy of ≃ 207 GeV as function of $\mathrm{m_H}$.

The decay of the Higgs boson into a fermion-antifermion pair is determined by the Yukawa coupling, $g_{\mathrm{Hf\bar{f}}}$, which is proportional to the fermion mass. Hence the Higgs boson is expected to decay dominantly into the heaviest fermion-antifermion pair kinematically allowed. In the mass range accessible at LEP the decay into b-quarks is dominant, also the

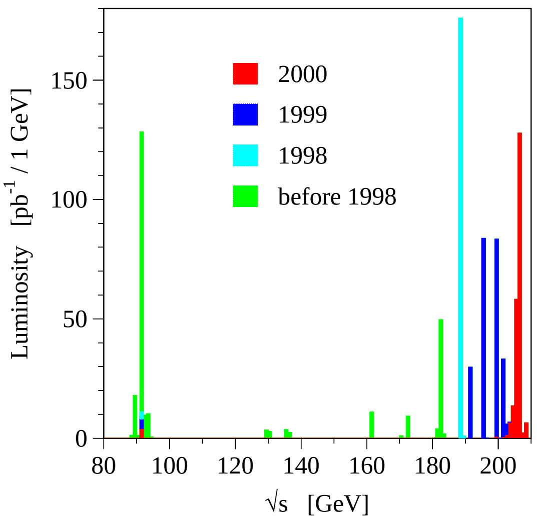

Figure 18: The integrated luminosities collected by all LEP experiments as function of $\sqrt{s}$. Of importance for the Higgs boson search at large m_H are the data with at the highest energies.

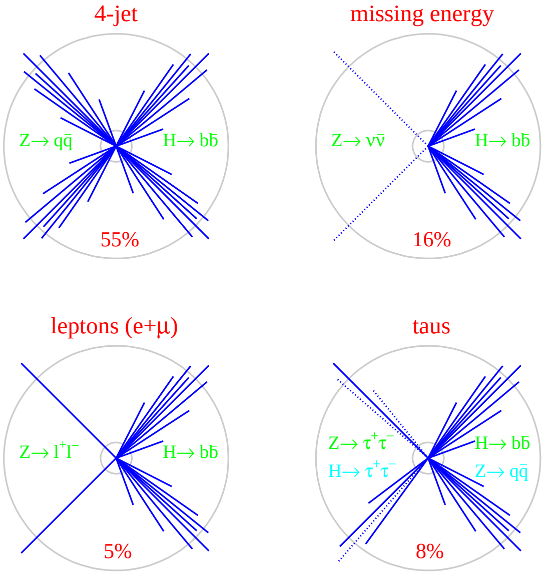

Figure 19: The event topologies for the dominant Higgs boson and Z decays

decay into a $\tau^+\tau^-$ is of importance. Taking into account the decay channels of the Z, the following final states must be considered: $ZH \rightarrow q\overline{q}b\overline{b}$, $ZH \rightarrow \nu\bar{\nu}b\overline{b}$, $ZH \rightarrow \ell^+\ell^-b\overline{b}$, and $ZH \rightarrow q\overline{q}\tau^+\tau^-$. They result into the event topologies shown in Figure 19. However, e^+e^- annihilation processes of large cross section, as shown in Figure 20, result in final states, which can fake a Higgs boson signal. In order to suppress the background and to isolate events originating from Higgs boson production dedicated techniques are developed. Of particular importance is the detection of b-quarks in jets assumed to stem from the Higgs boson. After hadronisation, b-quarks lead to B-hadrons in the jets with a lifetime τ_B of about 1.5 picoseconds. This lifetime is sufficient for a decay length of several mm, leading to secondary vertices. The reconstruction of the secondary vertices is achieved with silicon microvertex detectors. In addition, the presence of a Z is exploited requiring the invariant mass of the two jets not assigned to the Higgs boson or the two leptons to be equal to m_Z. Other quantities used to discriminate signal from background are event shape variables, characterising the kinematics of the jets, or boson production angles.

At the end of the analysis chain usually a few events remain which are in their features similar to the expected signal. The fraction of expected background and signal events is estimated from MC simulations. In order to gain sensitivity, the results of the four LEP experiments

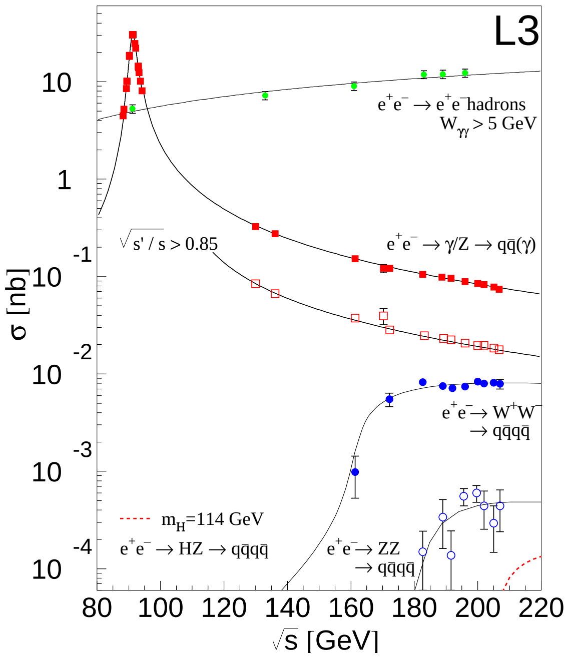

Figure 20: The cross sections of the main background processes in the Higgs boson search. For illustration, the expected cross section for a Higgs boson with $m_H = 114$ GeV is indicated as dashed line in the lower right edge.

are combined [32]. For that purpose to each selected event a weight is assigned which is obtained in the following way: The event characteristics important for the detection of a Higgs boson signal are used to construct a discriminant. For each channel the selected events are distributed as function of the discriminant. Events from all background processes and from the expected signal, which survive the analysis, are distributed in the same discriminant. For each bin of the distribution the ratio signal/background (S/B) is calculated, and this quantity is used to calculate the weight of the data events in the same bin of the distribution. As an example, Figure 21 shows the distribution of the invariant mass of the jets assigned to the Higgs boson for data, MC background and an expected signal with $m_H = 115$ GeV for an event sample with $S/B > 0.5$[5]. As can be seen data follow the distribution expected from the background. Finally, dedicated statistical analysis is applied to test the compatibility of the observed data with the expectation for only background and signal plus background hypotheses. The crucial

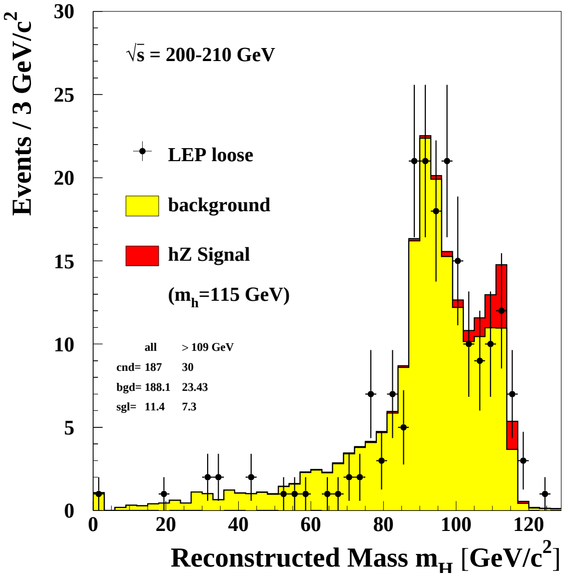

Figure 21: The invariant mass of the two jets assigned to the Higgs boson for data, background and signal events requiring S/B> 0.5. The mass of the Higgs boson is set to $m_H = 115$ GeV [32].

---

[5] This sample is obtained after application of cuts on the most sensitive quantities with no or only litle dependence on m_H.

quantity is the likelihood ratio

$$Q(\mathrm{m_H}) = \frac{\mathcal{L}(S+B)}{\mathcal{L}(B)}.$$

The logarithm of Q reads:

$$-2\ln Q(\mathrm{m_H}) = \\ 2s_{tot} - 2\sum_i N_i(1+\frac{S_i}{B_i}).$$

The index i runs over all bins of the discriminant distribution, s_{tot} is the total expected signal rate and N_i the number of data events in the bin. The quantity $-2\ln Q(\mathrm{m_H})$ is shown in Figure 22 as function of $\mathrm{m_H}$. The dashed line shows the expectation for the background, the dashed-dotted line for a signal plus background and the full line the result for the data. The dotted line is expected if a Higgs boson with $\mathrm{m_H}$ = 115 GeV would be present. There is some excess in data around $\mathrm{m_H}$ = 115 GeV with a statistical significance of 2.1 σ. This effect is due to an excess in the four-jet topology and these events originate mainly from the ALEPH experiment.

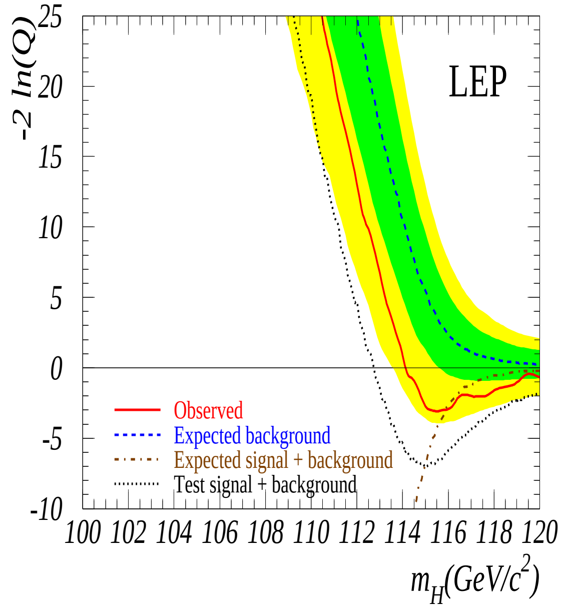

Figure 22: The quantity $-2\ln Q(\mathrm{m_H})$ obtained from the Higgs boson search results of all LEP experiments combined as function of $\mathrm{m_H}$. The dark and light grey areas indicate the 1σ and 2σ significances.

Since no significant signal is found the data are used to set a mass limit for the Higgs boson, exploiting the strong dependence of the Higgs boson production cross section on $\mathrm{m_H}$ shown in Figure 17. Taking again the results from all four experiments this lower mass limit is $\mathrm{m_H} >$ 114.1 GeV (95 % C.L.).

9.3. Supersymmetry

Supersymmetry is a tempting theoretical concept [33], which avoids the so called 'hierarchy problem' [34] and includes in a natural way gravity. It predicts supermultiplets which contain particles of different spins; *e.g.* the SM fermions of a $SU(2)$ doublet or singlet are supplemented by scalar 'sfermions' and the bosons by spin $\frac{1}{2}$ particles denoted vinos, zinos, higgsinos and gluinos. Gravitons with spin 2 are grouped with gravitinos of spin $\frac{3}{2}$. Unbroken supersymmetry would add, apart of many new particles, only one free parameter to the SM, called $\tan\beta = \frac{v_1}{v_2}$, where v_1 and v_2 are the vacuum expectation values of two Higgs doublets. Apparently supersymmetry is broken and supersymmetric particles are of larger mass than their ordinary partners in the multiplet. The mechanism of 'symmetry breaking' is unknown. Several mechanism are proposed and introduce many new parameters [36].

In supersymmetric models the Higgs sector contains at least two scalar dublets [35], resulting in 5 physical Higgs bosons. Two neutral ones, h and H, are CP even, one neutral A is CP odd and two, $\mathrm{H}^{\pm}$, are charged. Mixing between the two CP even eigenstate introduces a mixing angle α. The production of the lightest Higgs boson h proceeds either like in the SM in association with a Z or in association with the CP odd A. The couplings depend on α and β;

$$\begin{aligned} \frac{g_{\mathrm{ZZh}}}{g_{\mathrm{ZZH}}^{\mathrm{SM}}} &= \sin(\beta-\alpha) \\ \frac{g_{\mathrm{ZhA}}}{g_{\mathrm{ZZH}}^{\mathrm{SM}}} &= \cos(\beta-\alpha), \end{aligned}$$

where $g_{\mathrm{ZZH}}^{\mathrm{SM}} = \frac{1}{4}(g^2 + g'^2)v_0$ denotes the ZZH coupling in the SM. The decay into the $\mathrm{b\overline{b}}$ final state also depends on these parameters:

$$\begin{aligned} \frac{g_{\mathrm{hb\overline{b}}}}{g_{\mathrm{b\overline{b}}}^{\mathrm{SM}}} &= -\frac{\sin\alpha}{\cos\beta} \\ \frac{g_{\mathrm{Ab\overline{b}}}}{g_{\mathrm{b\overline{b}}}^{\mathrm{SM}}} &= \tan\beta, \end{aligned}$$

where $g_{\mathrm{b\overline{b}}}^{\mathrm{SM}} = g_{\mathrm{Hb\overline{b}}}$ is the Yukawa coupling. The masses of the Higgs bosons are related to each other and to the masses of the gauge bosons. In particular, the mass of the lightest Higgs boson, $\mathrm{m_h}$, is predicted to be smaller than $\mathrm{m_Z} \cdot |\cos 2\beta|$. Radiative corrections, depending strongly on the top-quark mass and the mixing of the scalar partners of the left- and right-handed top, shift $\mathrm{m_h}$ to larger values [37]. Both processes, $\mathrm{e^+e^-} \rightarrow \mathrm{h\,Z}$ and $\mathrm{e^+e^-} \rightarrow \mathrm{h\,A}$, are searched for at LEP using similar techniques as for the search of the SM Higgs boson. No signal is found, and exclusion limits are determined as function of $\tan\beta$. This is shown in Figure 23 [38] in the so called 'm$_\mathrm{h}$ max' scenario, in which the upper theoretical bound on $\mathrm{m_h}$ becomes maximal. Independent of $\tan\beta$, the mass limits for neutral Higgs bosons in the MSSM are set to $\mathrm{m_h} >$ 91.0 GeV and $\mathrm{m_A} >$ 91.9 GeV. No signal of charged Higgs bosons, charginos, neutralinos or sfermions were found at LEP and limits on their masses or production cross sections are set [39].

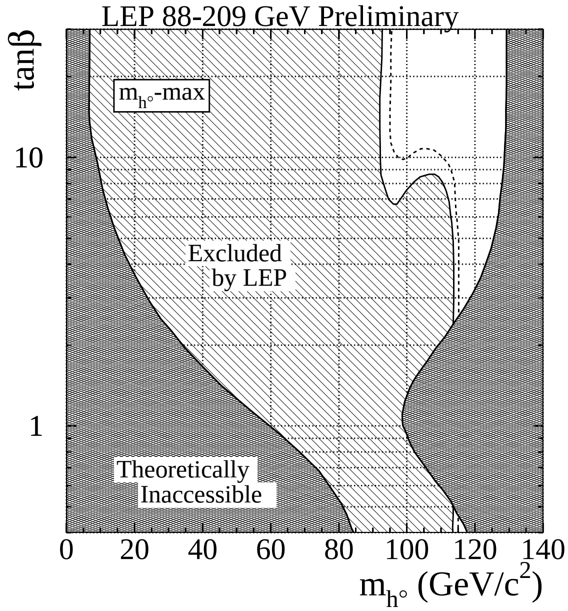

Figure 23: The excluded region in the $\mathrm{m_h}$-$\tan\beta$ plane in the 'm$_\mathrm{h}$ max'. The results of all LEP experiments are combined.

10. The TESLA project

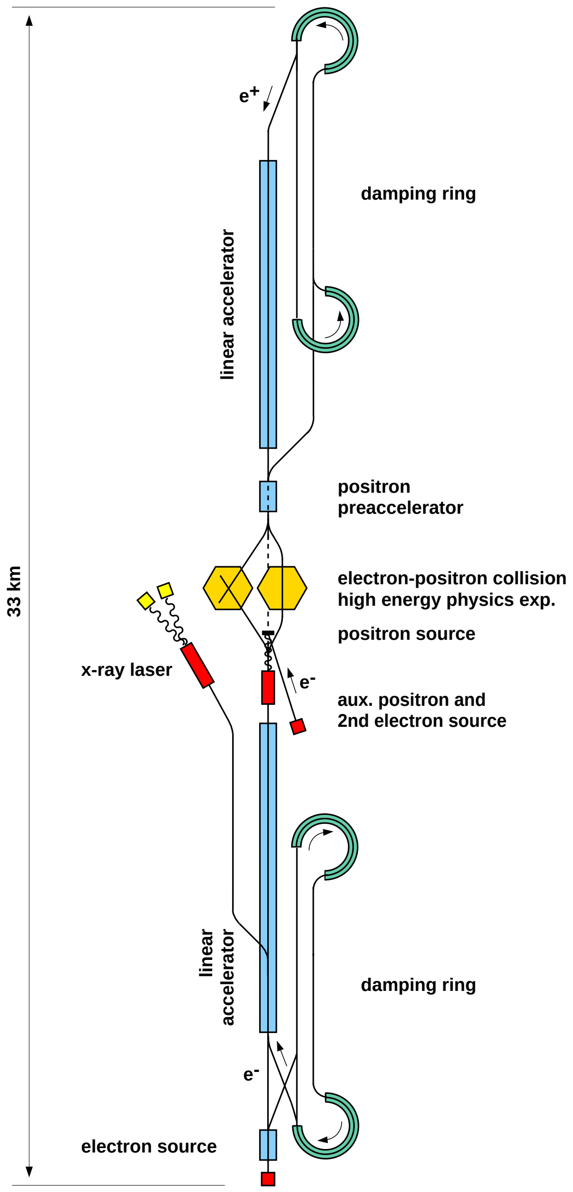

Figure 24: The layout of the TESLA linear collider at DESY

The LEP collider approached the technical frontier of a circular electron accelerator. The energy loss of the accelerated electrons per turn due to synchrotron radiation is $\Delta E \simeq {E_b}^4/R$, where E_b is the beam energy and R the radius of the accelerator. At the highest LEP energies these losses reached with about 3 GeV per turn the limit of the RF power. For a linear collider such losses do not exist. The main problems here are the high gradient of the acceleration cavities, in order to get the required energy with a technically reasonable length of the accelerator, and the luminosity. Electron or positron bunches are brought into collision only once, hence the permanent creation of new beam particles allowing high beam intensities is an issue. The advantages of an $\mathrm{e}^+\mathrm{e}^-$ collider, in comparison to a proton machine, are the well defined initial state and the possibility to tune both $\sqrt{s}$ and the polarisation of electrons and positrons very precisely. Furthermore, also $\mathrm{e}^-\ \mathrm{e}^-$, $\mathrm{e}^-\gamma$ and $\gamma\gamma$ scattering are options to extend the physics potential. A linear $\mathrm{e}^+\mathrm{e}^-$ collider operated in the energy range below 1 TeV would allow to study triple gauge boson couplings on a precision level sensitive to new physics, would cover the threshold of $\mathrm{e}^+\mathrm{e}^- \to \mathrm{t}\bar{\mathrm{t}}$ production, and in particular, would be the ideal machine to explore the Higgs mechanism or any new particle discovered in the new energy domain. A sketch of the TESLA [8] linear collider, proposed by the DESY laboratory, is shown in Figure 24. The accelerator is foreseen to be constructed starting from the DESY site in Hamburg in north-

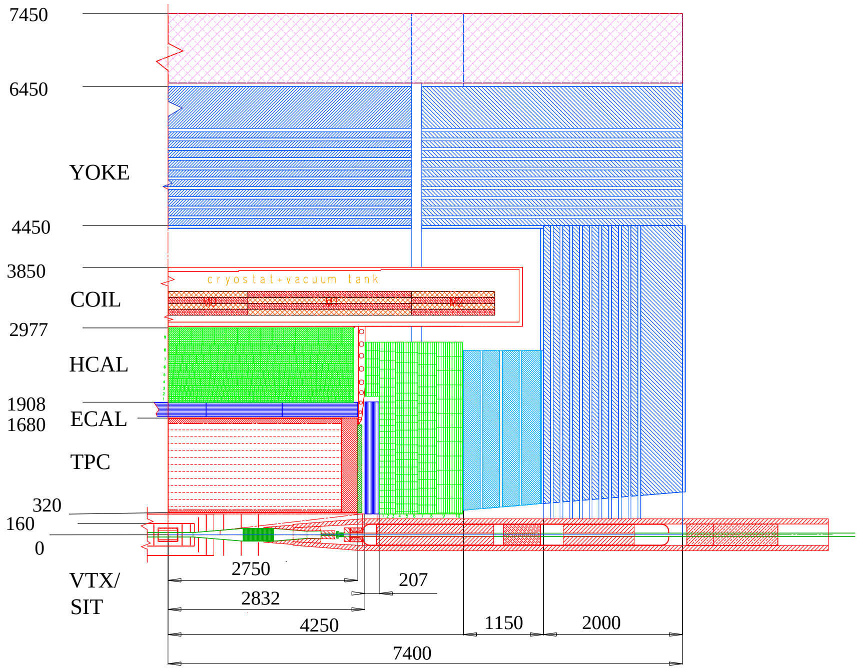

Figure 25: The layout of the detector for TESLA.

west direction. The total length will be about 30 km. The basic parameters of TESLA are:

$\sqrt{s}$	≤ 0.8 TeV
gradient	23.4 MeV/m
repetition rate	5 Hz
beam pulse length	950 μs
No. of bunches per pulse	2820
bunch spacing	337 ns
charge per bunch	$2 \cdot 10^{10}$
beam size, σ_x	553 nm
beam size, σ_y	5 nm
bunch length	0.3 mm
Luminosity	3.4 10^{34}cm^{-2}s^{-1}

In the interaction region one detector for the measurement of e^+e^- annihilations is foreseen. For a second detector, designed to measure $\gamma\gamma$ collision, an option exists. The feasibility of photon beams is under study. The detector, of which a quarter is depicted in Figure 25, follows in general the structure of a LEP detector. Starting from the interaction point there is a silicon tracker (VTX/SIT), a Time Projection Chamber (TPC) as the main tracking device, an electromagnetic (ECAL) and a hadron (HCAL) calorimeter. All these subdetectors are housed in a superconducting solenoidal magnet of 3 T. Much better in comparison to the LEP detectors are, however, the performances of the subdetectors. The envisaged momentum resolution is $\frac{\sigma_{p_t}}{p_t} = 4 \cdot 10^{-5} \cdot p_t$ [GeV], the impact parameter resolution $\sigma = 2.9 \oplus \frac{3.9}{p \cdot sin^{3/2}\theta)}\mu$m, the resolution of the energy measurement in the electromagnetic calorimeter $\frac{\sigma_{E_{el}}}{E_{el}} = \frac{11\%}{\sqrt{E_{el}}} + 0.6\%$ and in the hadron calorimeter $\frac{\sigma_{E_h}}{E_h} = \frac{35\%}{\sqrt{E_h}} + 3\%$.

11. Physics

The cross sections of e^+e^- annihilations in different final states as function of the centre-of-mass energy are shown in Figure 26. Choosing *e.g.* $\sqrt{s} = 350$ GeV and an integrated Luminosity of 500 fb^{-1} in one year of running the following event numbers are expected:

process	No. of events
$e^+e^- \to e^+e^-$	$1.5 \cdot 10^8$
$e^+e^- \to W^+W^-$	$5 \cdot 10^6$
$e^+e^- \to q\overline{q}$	$3 \cdot 10^6$
$e^+e^- \to \mu^+\mu^-$	$5 \cdot 10^5$
$e^+e^- \to ZZ$	$4 \cdot 10^5$
$e^+e^- \to Z\,H$	$8 \cdot 10^4$

($m_H = 120$ GeV)

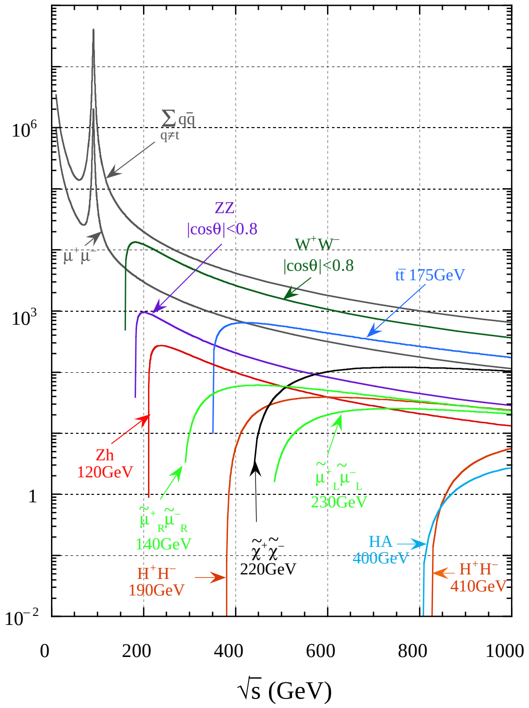

Figure 26: The cross sections of e^+e^- annihilations in several final states as expected in the $\sqrt{s}$ range of TESLA. Also shown are the expectations for the production of supersymmetric particles for given masses.

With such a statistics many measurements done at LEP can be performed at higher energy with considerably better accuracy [8]. Cross section measurements of $e^+e^- \to f\,\bar{f}$ will be sensitive to contact interactions up to several 10 TeV. Up to the same mass scale extra dimensions [40] can be probed. The study of $e^+e^- \to W^+W^-$ will allow to determine the triple gauge boson couplings, $\Delta\kappa$ and Δg_1^Z, with an accuracy of $\sim 10^{-4}$. This is of particular interest, since radiative corrections to these quantities in the framework of supersymmetry amount to $\sim 10^{-3}$. A comparison of the accuracies obtained for $\Delta\kappa_\gamma$ at LEP and expected at LHC and TESLA at $\sqrt{s} = 500$ GeV and $\sqrt{s} = 800$ GeV is shown in Figure 27. Another important issue is the study of the process $e^+e^- \to t\bar{t}$, which is accessible for the first time. From a threshold scan, the top-quark mass, m_t, will be determined with an accuracy of $\simeq 30$ MeV. Other topics are the couplings of the top-quark to gauge bosons, the Lorentz-structure in top-quark decays and the top-quark Yukawa coupling to the Higgs boson. The principal subject will be, however, the Higgs boson. The precision measurements at LEP and SLC on the Z point to a light Higgs boson, which will be accessible at TESLA. Due to the high event statistics expected, detailed studies of the profile of the Higgs boson

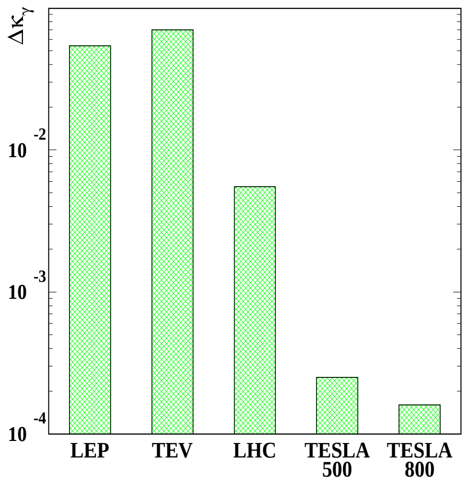

Figure 27: The error on $\Delta\kappa_\gamma$ obtained at LEP and the expectation for the LHC and TESLA. At TESLA estimates for $\sqrt{s} = 500$ GeV and $\sqrt{s} = 800$ GeV are given [8].

will be possible. This is discussed now in more detail.

12. Higgs Boson

The cross section for the two dominant processes of Higgs boson production, the Higgs-strahlung and the WW fusion [41], read:

$$\sigma(\mathrm{Z\,H}) = \frac{g^2_{\mathrm{ZZH}} G_{\mathrm{F}}(v_e^2 + a_e^2)}{96\sqrt{2}\pi s} \times\beta\frac{\beta^2 + 12\mathrm{m_Z}^2/s}{(1-\mathrm{m_Z}^2/s)^2}$$

$$\sigma(\nu\bar{\nu}\mathrm{H}) \simeq \frac{g^2_{\mathrm{WWH}}}{4\pi}\frac{G_{\mathrm{F}}^2}{8\pi^2}((1+\frac{\mathrm{m_H^2}}{s}) \times\log\frac{s}{\mathrm{m_H^2}} - 2(1-\frac{\mathrm{m_H^2}}{s})),$$

where $g_{\mathrm{ZZH}} = \frac{1}{4}(g^2 + g'^2)\upsilon_0$ and $g_{\mathrm{WWH}} = \frac{1}{2}g'^2\upsilon_0$. These cross sections are depicted as function of $\mathrm{m_H}$ for several $\sqrt{s}$ in Figure 28. The decay into fermions and bosons is described as:

$$\Gamma(\mathrm{H}\to\mathrm{f\,\bar{f}}) = \frac{g^2_{\mathrm{Hf\,\bar{f}}}}{4\pi}\frac{N_c}{2}\mathrm{m_H} \times(1-4\mathrm{m_f^2}/\mathrm{m_H^2})^{\frac{3}{2}}$$

and

$$\Gamma(\mathrm{H}\to\mathrm{VV}) = \frac{g^2_{\mathrm{VVH}}}{4\pi}\frac{3}{8\mathrm{m_H}}(1-\frac{\mathrm{m_H^2}}{3\mathrm{m_V^2}} +\frac{\mathrm{m_H^4}}{12\mathrm{m_V^4}})(1-4\mathrm{m_V^2}/\mathrm{m_H^2})^{\frac{1}{2}},$$

where V = W or Z. Using these formulae the branching fractions of the Higgs boson in the several final states are calculated [6] and shown in Figure 29. For

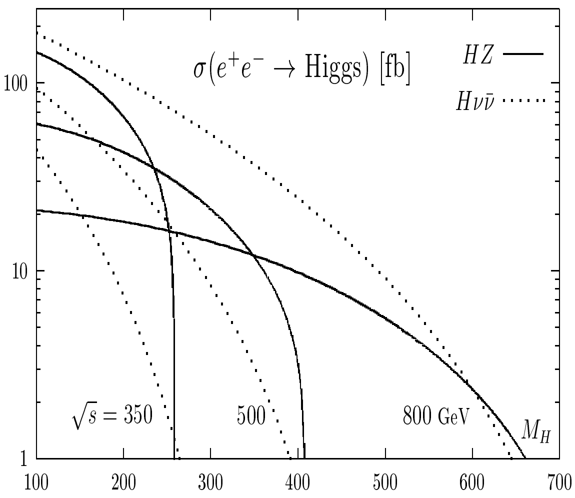

Figure 28: The cross section of Higgs-strahlung and WW fusion as function of $\mathrm{m_H}$ for $\sqrt{s} = 350, 500$ and 800 GeV [8].

---

[6] The decays $\mathrm{H}\to\gamma\gamma$ and $\mathrm{H}\to\mathrm{gg}$ are possible via quark loops.

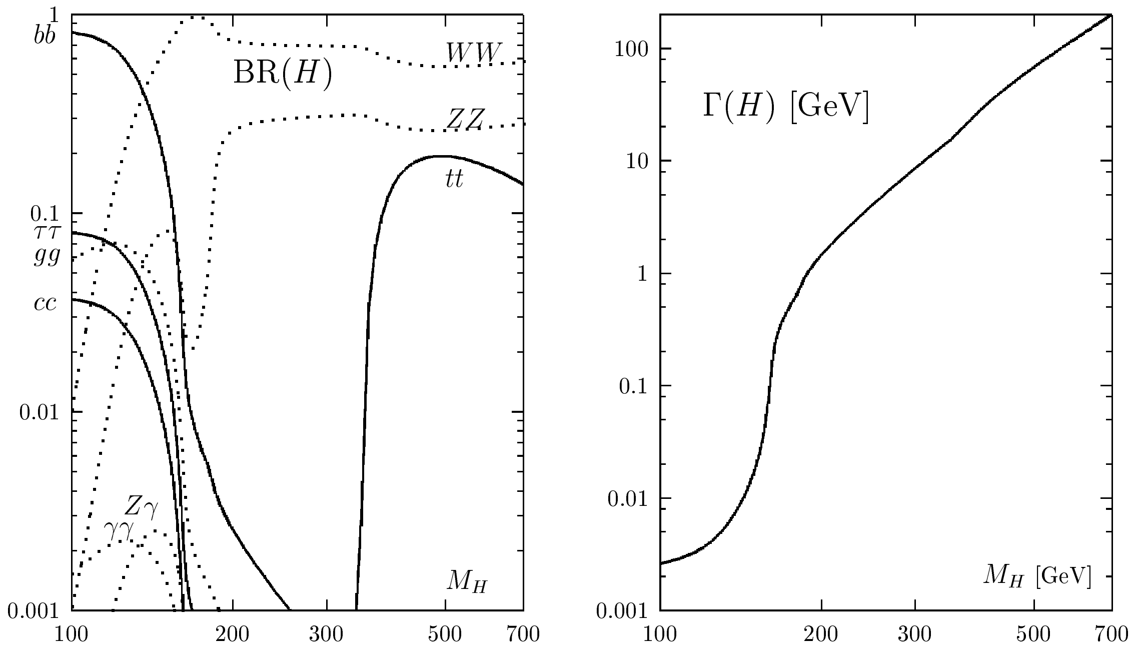

Figure 29: The branching fractions of the Higgs boson into fermions and bosons as function of m_H (left). The total width of the Higgs boson as function of m_H (right) [8].

$\sqrt{s} \simeq 350$ GeV and a m_H range from 100 to 200 GeV the dominant production mechanism will be Higgs-strahlung with substantial contribution from WW fusion, and the dominant decay modes will be $H \to b\overline{b}$ for $m_H \simeq$100 GeV and $H \to W^+W^-$ for $m_H \simeq$200 GeV.

12.1. Mass and Width

The first quantity to be determined experimentally is clearly the Higgs mass. The most model independent way to measure m_H is using the recoil mass against the Z. The Z is identified by its decay into electrons and muons, and the recoil mass is obtained as

$$m_R{}^2 = s - 2 \cdot \sqrt{s} \cdot E_Z + m_Z{}^2.$$

E_Z is the energy of the Z reconstructed from the two leptons. Events of this topology have a very clear signature in the detector as shown in Figure 30. The spectrum of the recoil mass, m_R, is displayed in Figure 31 assuming m_H = 120 GeV. The Higgs boson appears as a very sharp and clear signal over a small background. The latter originates mainly from $e^+e^- \to ZZ$. The precision of m_H obtained from a fit to this distribution is 110 MeV. The accuracy of the mass measurement can be improved by using also the hadronic decay channels of the Z and performing a kinematic fit to the whole event requiring energy and momentum conservation. The invariant mass distribution of the two jets assigned

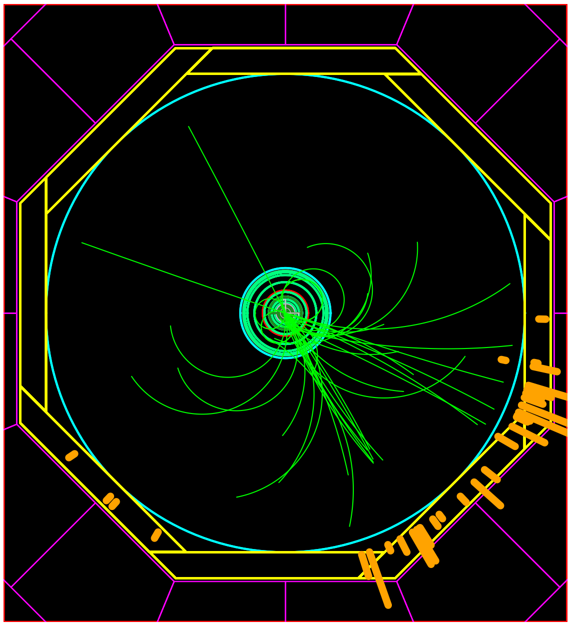

Figure 30: An event display for $e^+e^- \to ZH$ with $Z \to \mu^+\mu^-$ and $H \to b\bar{b}$. The isolated tracks of the two muons and the two b-quark jets are clearly visible.

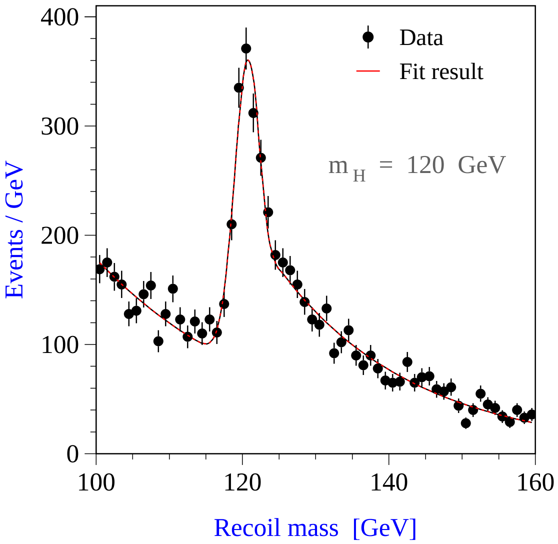

Figure 31: The distribution of the recoil mass against the Z in $e^+e^- \to ZH$ events and Z decays into electrons and muons assuming $m_H = 120$ GeV.

to the Higgs boson decay is shown in Figure 32. Also shown are the distributions obtained after the requirements that one or two jets contain a secondary vertex caused by a b-quark decay. This requirement supresses strongly the background whereas the signal stays nearly unchanged. The precision obtained for m_H is 45 MeV. If m_H approaches the W^+W^- threshold the decay $H \to W^+W^-$ becomes dominant and causes more complex final states. Using proper jet clustering algorithms the decay channels $ZH \to \ell^+\ell^-W^+W^-$ and $ZH \to q\bar{q}W^+W^-$ can be reconstructed. This is shown in Figure 33 for the channel $ZH \to q\bar{q}W^+W^-$ with six hadronic jets in the final state. The Higgs boson signal is very clear on top of a moderate background. The accuracy of the mass measurement is $\simeq 110$ MeV. Combining all channels the Higgs boson mass will be measured with an accuracy of $\simeq$ 40 MeV at $m_H \simeq 120$ GeV and $\simeq 70$ MeV at $m_H \simeq 180$ GeV.

The width of the Higgs boson, $\Gamma(H)$ is of several GeV for masses $m_H > 250$ GeV and the detector performance allows to measure it directly from the invariant mass distribution. At lower masses, however, the mass resolution is much larger than $\Gamma(H)$. But using the relation $\Gamma(H) = \frac{\Gamma(H\to X)}{\mathcal{B}(H\to X)}$, with $X = WW, ZZ$ or $\gamma\gamma$, the width can be determined indirectly. For example, the partial width of $H \to \gamma\gamma$ can be measured via Higgs boson production in a $\gamma\gamma$ collider. The branching fraction for $H \to \gamma\gamma$ is acces-

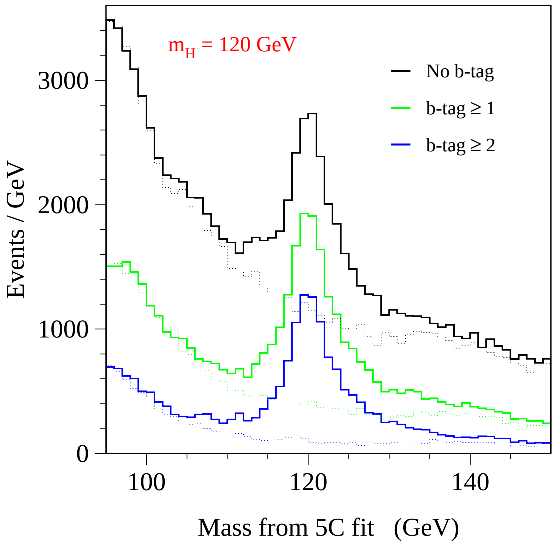

Figure 32: The invariant mass distribution of the two b-quark jets from $H \rightarrow b\bar{b}$ after imposing energy and momentum conservation and constraining the mass of the two jets assigned to the Z to m_Z [8].

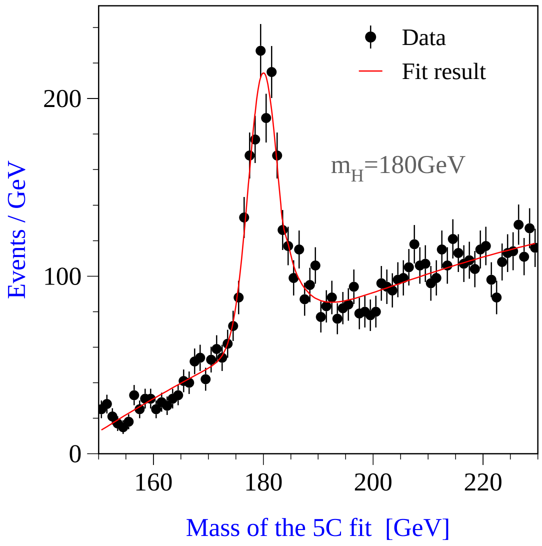

Figure 33: The invariant mass distribution of the four jets stemming from $H \rightarrow W^+W^-$ decays after imposing energy and momentum conservation and constraining the mass of the two jets assigned to the Z to m_Z [8].

sible in the e^+e^- collider by using the $\gamma\gamma$ invariant mass spectrum. The same exercise can be done for WW fusion and $H \rightarrow W^+W^-$. Depending on m_H, the width of the Higgs boson can be determined with an accuracy between 4 and 10%.

12.2. Branching Fractions

The branching fractions, as shown in Figure 29, are precisely predicted in the SM. In supersymmetric extensions of the SM they are presumably different. Hence its measurement is crucial to find out which structure of the Higgs sector is realised in nature. The measurement of branching fractions makes use of the mass distributions shown in the previous section and, in addition, uses the excellent flavour tagging capabilities of the detector. The result is shown in Figure 34.

12.3. Spin

If a signal is seen in the dijet invariant mass distribution the measurement of the spin is crucial for its identification as the Higgs boson. It can be performed by analysing the energy dependence of the Higgs boson production cross section just above the kinematic threshold. For a spin zero particle the rise of the cross section is expected to be $\sim \beta$, where β is the velocity of the boson in the centre-of-

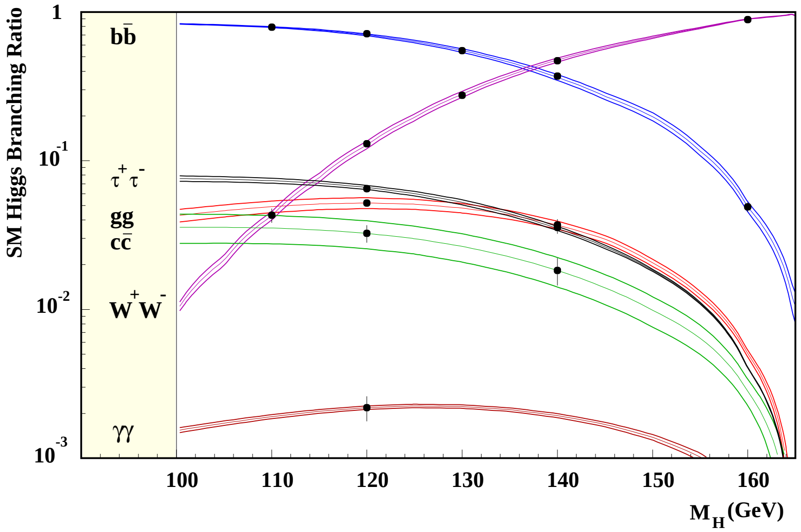

Figure 34: The measured branching fractions of the Higgs boson into fermions and bosons as function of m_H. Dots are measurements and the curves the predictions by the SM [8].

mass system [7]. For a spin one particle the rise is $\sim \beta^3$ and for spin two like $\sim \beta^5$. With a very small luminosity of about 20 fb^{-1} per energy point the scalar nature of the Higgs boson can be established, as shown in Figure 35.

12.4. Self Couplings

From the potential in the Lagrangian terms remain which describe triple and quartic self couplings of the Higgs boson. The measurement of these couplings would specify the Higgs potential containing the parameters v_0 and λ. The triple Higgs boson couplings appear in the Feynman-diagram depicted in Figure 36. At TESLA, asuming $\sqrt{s}$ = 500 GeV and an integrated luminosity of 1 ab^{-1}, the triple Higgs boson couplings can be detected. This is demonstrated in Figure 37. A measurement of λ is feasible at $\sqrt{s}$ = 500 GeV with an accuracy of $\simeq$ 20%.

13. Summary

From measurements at LEP the parameters of the heavy neutral gauge boson, Z, were precisely determined. The SM was confirmed on the level of quantum corrections. At high LEP energies the triple gauge boson couplings, predicted by the non-abelian structure of the SM, were detected and found to be in agreement with the prediction. The Higgs boson, the missing key-stone of the SM, was not found. But from direct searches and from virtual Higgs boson contributions to

---

[7] There are particular scenarios for s=1 and 2, which show a threshold behaviour similar in shape to the s=0 one. This can be disentangled using angular information in addition.

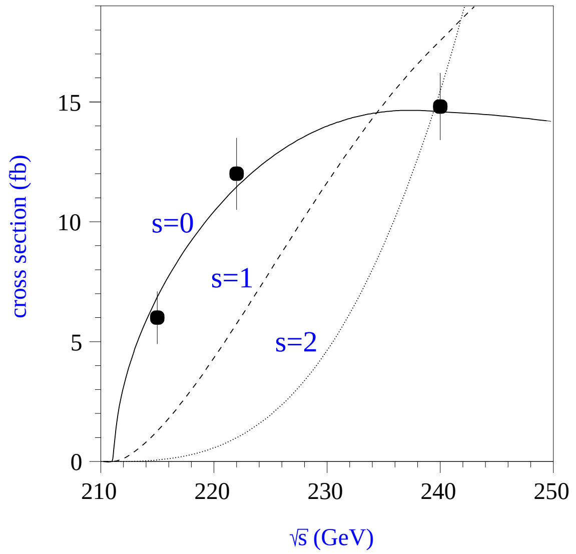

Figure 35: The cross section of $e^+e^- \rightarrow ZH \rightarrow \ell^+\ell^- + 2$-jet just above the threshold assuming $m_H = 120$ GeV. The dots correspond to a measurement and the curves are predictions for several spins [8].

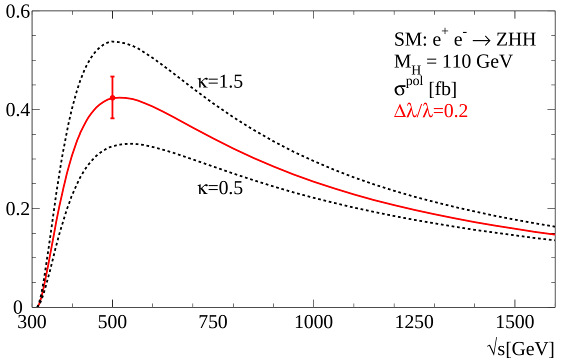

Figure 37: The energy dependence of the cross section of $e^+e^- \rightarrow ZZH$ for $m_H = 110$ GeV. The dot represents a measurement, the full line the expectation from the SM and the dashed line the prediction obtained if the SM cross section of the triple Higgs coupling contribution is multiplied by κ [8].

observables its mass is estimeted to be between 114 and $\simeq 200$ GeV. The TESLA collider offers an excellent physics program to confirm or disprove the SM in a new energy domain. In particular the profile of the Higgs particle, its mass, spin, and couplings, will allow to explore the mechanism of spontaneous symmetry breaking. The top-quark, the heaviest elementary particle known so far, will be subject to detailed studies. Precision measurements on fermion couplings to gauge bosons, triple and also quartic gauge boson self-couplings will give us hints for new physics beyond the SM. And of course, a new energy domain will be explored, eventually being full of unexpected phenomena.

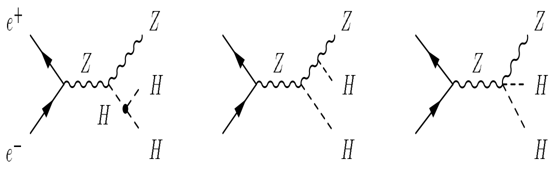

Figure 36: The Feynman-diagrams describing the triple Higgs self coupling (left) and two background contributions of similar topology (right) .

Acknowledgements

I would like to thank the organisers of the school for their kind hospitality and K. Mönig, A. Raspereza, S. Riemann and A. Stahl for the critical reading of the text.

References

[1] H. U. Martyn, "Test of QED in e^+e^- collisions", in *Quantum Electrodynamics*, edited by T. Kinishita, World Scientific, (1990).

[2] F. J. Hasert *et al.*,*Phys. Lett.* B **46**, 121 (1973).

[3] G. Arnison *et al.*,*Phys. Lett.* B **122**, 103 (1983), *Phys. Lett.* B **134**, 469 (1984), M. Banner *et al.*, *Phys. Lett.* B **122**, 476 (1983), P. Bagnania *et al.*, *Z. Phys.* C **24**, 1 (1984).

[4] S. L. Glashow,*Nucl. Phys.* **22**, 579 (1961), S. Weinberg, *Phys. Rev. Lett.* **19**, 1264 (1967), A. Salam, "Weak and Electromagnetic Interactions", in *Elementary Particle Theory*, edited by N. Svartholm, page 367, Stockholm, 1969, Almqvist and Wiksell.

[5] I. Wilson and H. Henke, CERN Yellow Report 89-09 (1989), S. Myers, CERN Yellow Report 91-08 (1991).

[6] J.K. Gaemers *et al.*, *Z. Phys.* C **1**, 259 (1979), K. Hagiwara *et al.*, *Nucl. Phys.* B **282**, 253 (1987).

[7] P. W. Higgs, *Phys. Lett.* **12**, 132 (1964), F. Englert and R. Brout, *Phys. Rev. Lett.* **13**, 321 (1964), G. S. Guralnik et al., *Phys. Rev. Lett.* **13**, 585 (1964).

[8] TESLA Technical Design Report, DESY 2001-011 and References quoted therein.

[9] ALEPH Coll. *Nucl. Instrum. Methods* **294**, 121 (1990), DELPHI Coll. *Nucl. Instrum. Methods* **303**, 233 (1991), L3 Coll. *Nucl. Instrum. Methods* **289**, 35 (1990), OPAL Coll. *Nucl. Instrum. Methods* **305**, 275 (1991).

[10] CODATA Recommended Values, P. J. Mohr and B. N. Taylor, Rev. Mod. Phys. **72** 351 (2000).

[11] D. E. Groom *et al.*,*Eur. Phys. Jour.* C **15**, 1 (2000).

[12] D. Bardin *et al.*, *Z. Phys.* C **44**, 493 (1989), *Nucl. Phys.* B **351**, 1 (1991), DESY 99-070.

[13] G. Montagna *et al.*, *Nucl. Phys.* B **401**, 3 (1993), G. Montagna *et al.*, *Comput. Phys. Comm.* **117**, 278 (1999).

[14] OPAL Coll.,*Eur. Phys. Jour.* C **19**, 587 (2001).

[15] The LEP electroweak working group, CERN-EP/2001-021 and LEPEWWG 2001-02.

[16] DELPHI Coll.,*Eur. Phys. Jour.* C **16**, 371 (2000).

[17] L3 Coll., *Phys. Lett.* B **429**, 387 (1998).

[18] SLD Coll., *Phys. Rev. Lett.* **84**, 5945 (2000).

[19] S. Eidelmann and F. Jegerlehner, *Z. Phys.* C **67**, 585 (1995), H. Burkhardt and B. Pietrzyk, LAPP-EXP 2001-03.

[20] M. Veltman, *Nucl. Phys.* B **123**, 89 (1977), J. Fleischer and F. Jegerlehner,*Nucl. Phys.* B **228**, 1 (1983).

[21] A. Sirlin, *Phys. Rev.* D **22**, 971 (1980), A. A. Akhundov *et al.*, *Nucl. Phys.* B **276**, 1 (1986).

[22] M. Veltman,Acta Phys. Polon. B8, 475 (1977).

[23] The LEP electroweak working group, CERN/PPE/93-157.

[24] CDF Coll. *Phys. Rev. Lett.* **73**, 225 (1994), *Phys. Rev.* D **50**, 2966 (1994).

[25] http://www-cdf.fnal.gov/ physics/ewk/wmass_new.htm, K. McFarland, hep-ex/ 9806013.

[26] L. Demortier *et al.*, FERMILAB-TM-2084, (1999).

[27] S.G. Porsev *et al.*, *Phys. Rev. Lett.* **86**, 3260 (2001).

[28] The LEP electroweak working group, 2f subgroup, LEP2ff/01-02.

[29] E.J. Eichten *et al.*,*Phys. Rev. Lett.* **50**, 811 (1983).

[30] L3 Coll. L3 Note 2637, submitted to the EPS-HEP, Budapest 2001.

[31] LEP-TGC Working group, LEPEWWG/TGC/2000-02.

[32] The LEP Higgs working group, LHWG Note/2001-03, CERN-EP/2001-055.

[33] Yu. A. Gol'fand and E. P. Likhtman, *ZhETF Pis. Red.* 13 452 (1971), V. P. Akulov and D. V. Volkov, *Phys. Lett.* B **46**, 109 (1973), J. Wess and B. Zumino, *Nucl. Phys.* B **70**, 39 (1974).

[34] S. Weinberg, *Phys. Rev.* D **13**, 974 (1976), *Phys. Rev.* D **19**, 1277 (1979), L. Susskind, *Phys. Rev.* D **20**, 2619 (1979).

[35] P. Fayet, *Nucl. Phys.* B **90**, 104 (1975).

[36] A.H. Chamseddine *et al.Phys. Rev. Lett.* **49**, 970 (1982), L.J. Hall *et al.Phys. Rev.* D **27**, 2359 (1983), M. Dine *et al.*, *Phys. Rev.* D **48**, 1277 (1993), *Phys. Rev.* D **51**, 1362 (1995).

[37] S. Heinemeyer *et al.*, *Phys. Rev.* D **58**, 091701 (1998), *Phys. Lett.* B **440**, 296 (1998), *Eur. Phys. Jour.* C **9**, 343 (1999).

[38] The LEP Higgs working group, LHWG Note/2001-04.

[39] The LEP SUSY working group, LEPSUSY WG/01-01.1, LEPSUSY WG/01-02.1 and LEPSUSY WG/01-03.1.

[40] N. Arkani-Hamed *et al.*, *Phys. Lett.* B **373**, 135 (1996).

[41] J. Ellis *et al.*, *Nucl. Phys.* B **106**, 292 (1976), B. L. Ioffe and V. A. Khoze *Sov. J. Nucl. Phys.* **9**, 50, (1978), B.W. Lee *et al.*, *Phys. Rev.* **16**, 1519 (1977), D.R.T. Jones and S. Petcov, *Phys. Lett.* B **84**, 440 (1979), G. Kane *et al.*, *Phys. Lett.* B **148**, 367 (1984), G. Altarelli *et al.*, *Nucl. Phys.* B **287**, 205 (1987), W. Kilian *et al.*, *Phys. Lett.* B **373**, 135 (1996).